

## RESEARCH ARTICLE

## Urine metabolomics of rats with chronic atrophic gastritis

Guo-Xiu Zu<sup>1</sup>, Qian-Qian Sun<sup>1</sup>, Jian Chen<sup>1,2</sup>, Xi-Jian Liu<sup>1</sup>, Ke-Yun Sun<sup>1</sup>, Liang-Kun Zhang<sup>1</sup>, Ling Li<sup>1</sup>, Tao Han<sup>3\*</sup>, Hai-Liang Huang<sup>4\*</sup>

**1** Department of Traditional Chinese Medicine, Shandong University of Traditional Chinese Medicine, Jinan, Shandong, China, **2** Affiliated Central Hospital of Shandong First Medical University, Shandong First Medical University, Jinan, Shandong, China, **3** Graduate Office, Shandong University of Traditional Chinese Medicine, Jinan, Shandong, China, **4** Department of Rehabilitation Medicine, Shandong University of Traditional Chinese Medicine, Jinan, Shandong, China

\* These authors contributed equally to this work.

\* [60012002@sducm.edu.cn](mailto:60012002@sducm.edu.cn) (TH); [06000031@sducm.edu.cn](mailto:06000031@sducm.edu.cn) (HLH)

## OPEN ACCESS

**Citation:** Zu G-X, Sun Q-Q, Chen J, Liu X-J, Sun K-Y, Zhang L-K, et al. (2020) Urine metabolomics of rats with chronic atrophic gastritis. PLoS ONE 15 (11): e0236203. <https://doi.org/10.1371/journal.pone.0236203>

**Editor:** Tommaso Lomonaco, University of Pisa, ITALY

**Received:** June 30, 2020

**Accepted:** October 27, 2020

**Published:** November 11, 2020

**Peer Review History:** PLOS recognizes the benefits of transparency in the peer review process; therefore, we enable the publication of all of the content of peer review and author responses alongside final, published articles. The editorial history of this article is available here: <https://doi.org/10.1371/journal.pone.0236203>

**Copyright:** © 2020 Zu et al. This is an open access article distributed under the terms of the [Creative Commons Attribution License](https://creativecommons.org/licenses/by/4.0/), which permits unrestricted use, distribution, and reproduction in any medium, provided the original author and source are credited.

**Data Availability Statement:** All relevant data are within the paper and its [Supporting information](#) files.

**Funding:** The grant of the Preliminary Mechanism and Efficacy Evaluation by the excellent scientific

## Abstract

## Background/aim

To use liquid chromatography-mass spectrometry (LC-MS) to identify endogenous differential metabolites in the urine of rats with chronic atrophic gastritis (CAG).

## Materials and methods

Methylnitronitrosoguanidine (MNNG) was used to produce a CAG model in Wistar rats, and HE staining was used to determine the pathological model. LC-MS was used to detect the differential metabolic profiles in rat urine. Diversified analysis was performed by the statistical method.

## Results

Compared with the control group, the model group had 68 differential metabolites, 25 that were upregulated and 43 that were downregulated. The main metabolic pathways were D-glutamine and D-glutamic acid metabolism, histidine metabolism and purine metabolism.

## Conclusion

By searching for differential metabolites and metabolic pathways in the urine of CAG rats, this study provides effective experimental data for the pathogenesis and clinical diagnosis of CAG.

## Introduction

Chronic atrophic gastritis (CAG) is a type of atrophy of gastric mucosal epithelial cells and glands where the number of glands is reduced, the mucosal layer thins, and the mucosal

research and innovation teams at Shandong University of Traditional Chinese Medicine in the treatment of major diseases No. 220316 and Shandong province key research and development plan 2016CYJS08A01-6“Establishment of Clinical Diagnosis and Treatment Standard System of Precise Prescription for the Prevention and Treatment of Gastric Precancerous Lesions by Jingfang Pinellia Xiexin Decoction.

**Competing interests:** The authors have declared that no competing interests exist.

muscle layer thickens and may be accompanied by intestinal metaplasia and dysplasia. Digestive system diseases [1] mainly have the clinical manifestations of bloating, fullness of the stomach, belching, pain in the upper abdomen, loss of appetite, weight loss, etc. CAG has a wide variety of factors and is a common and frequently occurring clinical disease with a 2.55%- 7.46% canceration rate [2]. In 1978, the World Health Organization officially defined chronic atrophic gastritis as a precancerous state. The active treatment of CAG in clinical practice is an important node to block its development into gastric cancer.

As an important branch of systems biology, metabolomics technology is unique because it does not require the establishment of a large database of expressed gene sequences [3]. Metabolomics can express the physiological and biochemical state of the body through biological metabolic structure to better analyze pathogenesis. Among its advantages, liquid chromatography-mass spectrometry (LC-MS) technology can be directly used to analyze biological metabolites to obtain final analysis results with the advantage of finding subtle changes in gene and protein expression during biological metabolism. Thus, LC-MS has become the most commonly used analytical technique in metabolomics research [4]. This study explains the molecular mechanism of action and metabolic pathways of chronic atrophic gastritis through pharmacodynamics and LC-MS.

## Materials and methods

### Animals

Twenty SPF grade Wistar male rats, 6 weeks old,  $180 \pm 20$  g, were provided by Shandong Pengyue Experimental Animal Co., Ltd. [SCXK (Lu) 20140007]. The feeding environment was a temperature of  $26^{\circ}\text{C} \pm 2^{\circ}\text{C}$ , humidity  $50 \pm 10\%$ , and light illumination/dark cycle 12 h. The experiment started after 7 d of adaptive feeding from the time of purchase. During the period, the animals has free access to food and drinking water, and the experiment met animal ethical requirements.

### Experimental reagents and instruments

Methylnitronitrosoguanidine (manufactured by Tokyo Chemical Industry Co., Ltd., NH8JH-DR), vetzyme tablets (Lepu Hengjiuyuan Pharmaceutical Co., Ltd., 20170401), ranitidine hydrochloride capsules (Tianjin Pacific Pharmaceutical Co., Ltd., 20170601), and ammonium hydroxide (Shanghai Wokai Biotechnology Co., Ltd., 20170220) were used. Anhydrous ethanol (Tianjin Fuyu Fine Chemical Co., Ltd., 20170808), methanol (Woke), acetonitrile and formic acid (Aladdin), ammonium formate (Sigma), hematoxylin staining solution, eosin staining solution, differentiation solution, blue back solution (Hebei Bohai Biological Engineering Development Co., Ltd.), and xylene (Tianjin Yongda Chemical Reagent Co., Ltd.) were also utilized in this study.

A refrigerated centrifuge (Eppendorf, H1650-W), mixer (Vortex Mixer, QL-866), liquid chromatograph (Thermo, UltiMate 3000) and mass spectrometer Thermo (Q Exactive Focus) were instruments used in this study.

### Animal model

Twenty Wistar rats were prepared, and 10 rats were randomly selected as a blank group. Normal diet was fed until the materials were collected. The remaining rats were model rats according to the following method [5]: rats were given  $120 \mu\text{g}/\text{mL}$  MNNG from the 1st day of modeling, given 0.1% ammonia water freely for 24 h fed with 0.03% ranitidine feed using the hunger and satiety method (full food for 2 d, fasting for 1 d), an each given 2 ml of 40% ethanol

on the fasting day. The above operation lasted for 16 weeks and each rat was weighed twice a week during the modeling process. During the experiment, the weight, coat color and behavior of the rats were observed.

Example ethics statement: This study was carried out in strict accordance with the recommendations in the Guidelines for ethical review of experimental Animal welfare (National Standard: GB/T 35892–2018). The protocol was approved by the Ethics Review Center of Shandong University of Traditional Chinese Medicine (Protocol Number: SDUTCM20190402003). All surgery was performed under sodium pentobarbital anesthesia, and all efforts were made to minimize suffering.

### Urine collection and preparation

Before sampling, they fasted for 24 hours, drank normal water, collected urine, followed by anaesthesia with 2% pentobarbital sodium, blood collection of spleen, stomach and liver, and subsequent death. Urine was centrifuged at 2500 rpm at room temperature for 1 hour in the morning, and the supernatant was divided into centrifuge tubes; each tube was > 0.3 ml. The urine samples were melted at 4°C and 100 µL of each sample was placed into a 1.5 mL centrifuge tube, 100 µL of ddH<sub>2</sub>O was added followed by shaking for 5 min to fully absorb and centrifugation at 10000 g and 4°C for 10 min. Then, a 0.22 µm membrane was used to filter the supernatant to obtain the samples to be tested; 20 µL of the synthetic QC samples were extracted from each sample to be tested, and the remaining samples were tested by LC-MS.

### LC-MS chromatographic mass spectrometry conditions

A Thermo Ultimate 3000 chromatograph and an ACQUITY UPLC<sup>®</sup> HSS T3 1.8 µm (2.1 × 150 mm) chromatographic column were used with an autosampler temperature of 8°C, a flow rate of 0.25 mL/min, and a column temperature of 40°C. The sample was eluted with an injection volume of 2 µL, and the positive mode mobile phases were 0.1% formic acid in water (A) and 0.1% formic acid in acetonitrile (B). The gradient elution program was 0 ~ 2 min, 2% B; 2 ~ 10 min, 2% ~ 50% B; 10 ~ 15 min, 50% ~ 98% B; 15 ~ 20 min, 98% B; 20 ~ 22 min, 98% ~ 2% B; 22 ~ 25 min, 2% B. The negative mode mobile phases were 5 mM ammonium formate (A) and acetonitrile (B). The gradient elution program was 0 ~ 2 min, 2% B; 2 ~ 10 min, 2% ~ 50% B; 10 ~ 15 min, 50% ~ 98% B; 15 ~ 20 min, 98% B; 20 ~ 22 min, 98% ~ 2% B; 22 ~ 25 min, 2% B [6]. The Thermo Q Exactive Focus mass spectrometer was operated with the following conditions: electrospray ion (ESI) source, positive and negative ion ionization mode, positive ion spray voltage of 3.50 kV, negative ion spray voltage of -2.50 kV, sheath gas of 30 arb, auxiliary gas of 10 arb, capillary temperature of 325°C, full scan with a resolution of 70,000, scan range of m/z 81–1000, secondary cracking with HCD, collision voltage of 30 eV, and dynamic exclusion to remove unnecessary MS/MS information.

### Data processing

The analysis software used for multidimensional statistical analysis is SIMCA-P (V13.0). In addition, the calculation of P value is t-test. The t-test that we use for univariate statistical analysis, in general, t-test is p < 0.05 is significant, p < 0.01 is very significant, biological statistical methods are basically such a display of differences; This section provides references for significance of biological repeated screening p values. The obtained raw data was converted to mzXML format with ProteoWizard software (v3.0.8789) [7] and the RCMS (v3.3.2) XCMS package was used for peak identification, peak filtering, and peak alignment analysis. The main parameters were bw = 5, ppm = 15, peakwidth = c (10, 20), mzwid = 0.015, mzdiff = 0.01, and method = centWave, which includes the mass to charge ratio (m/z) and information data

matrix such as retention time (rt) and intensity. According to the results, the original peak area, which is the relative strength value, is calculated, then the original peak area is standardized, batch normalization of peak area of data. Data analysis is based on standardized data. Multidimensional statistical analysis was performed based on the data after standardized processing.

LC-MS data is carried out on the basis of normalization, eliminating very few data that do not exist or have too low strength. The experiment adopts most data retained after QC, QA and normalization processing. Prior to urine metabolomics analysis, the Proteowizard software (V3.0.8789) was used to convert the obtained original data into mzXML format (XCMS input file format). Using R (v3.3.2) XCMS package is used to identify the peaks identification, peaks filtration, peaks alignment, the main parameters are  $bw = 5$ ,  $PPM = 15$ ,  $peakwidth = c(10, 20)$ ,  $mzwid = 0.015$ ,  $mzdiff = 0.01$ , the method = centWave. The data matrix, including mass to charge ratio (M/Z), retention time (RT) and intensity, is obtained. In the positive ion mode 22,540 precursor molecules and the negative ion mode 18,837 precursor molecules were obtained. The data were exported to Excel for subsequent analysis. In order to make comparison of data of different orders, batch normalization of data regarding peak area was conducted.

## Results

### General situation

Control group: In good condition, sturdy body, strong limbs, neat, supple and shiny fur, mental state is excellent, responsive to external conditions, body weight gradually increases, and the stool is normal. Model group: Poor condition, thin body, weak limbs, messy fur, dryness, and dullness, poor mental state, drowsiness, unresponsive to external conditions, insignificant changes in body mass, slower rise, and less stool that is hard. Body mass changes are shown in Fig 1. In the registration of weight changes at 16 weeks, normality test was performed first, and then one-way ANOVA was used to conduct statistical test of weight between the blank group and the model group, and  $*P < 0.01$  was found between the two groups, the difference was statistically significant.

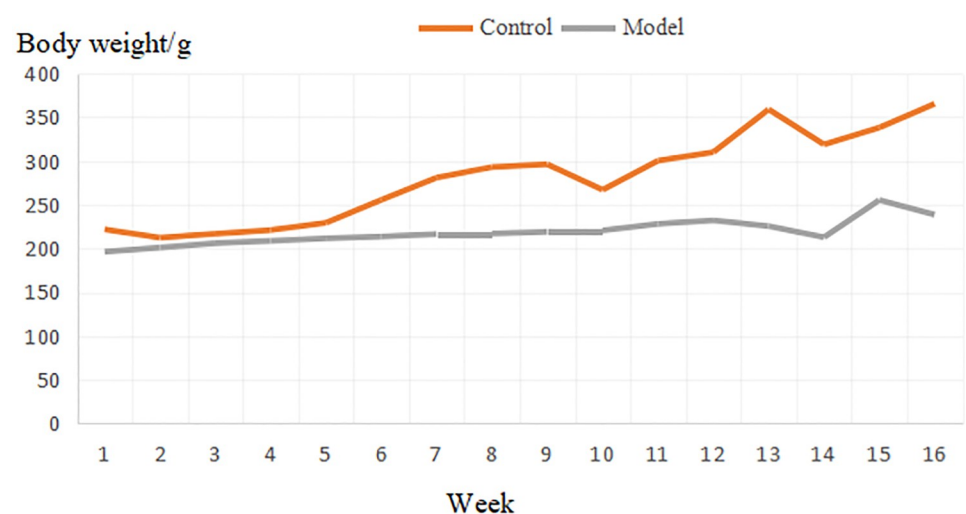


**Fig 1. Mass variation diagram of the control group and model group.**

<https://doi.org/10.1371/journal.pone.0236203.g001>

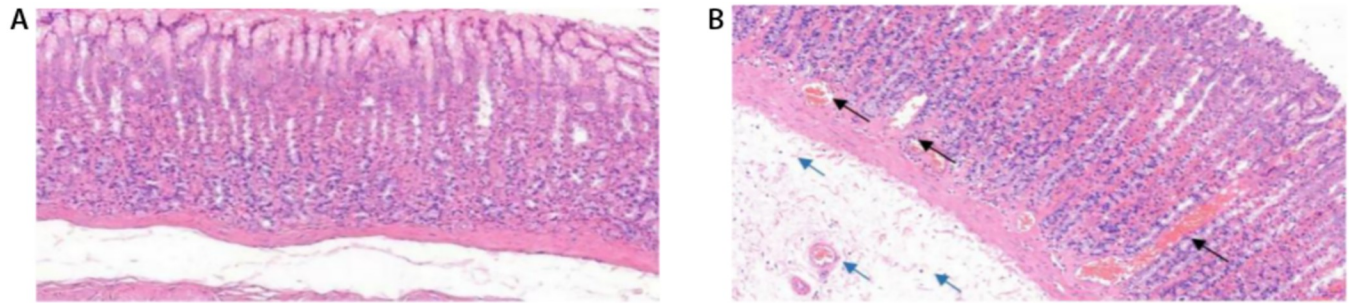


**Fig 2. HE staining pathological sections.** A. HE Staining Pathological Sections of Gastric Mucosa in the Control Group ( $\times 200$ ); 2-B: HE Staining Pathological Sections of Gastric Mucosa in the Model Group ( $\times 200$ ).

<https://doi.org/10.1371/journal.pone.0236203.g002>

### Observation of pathological tissues

As shown in Fig 2A, the gastric tissue mucosa lamina propria in the blank group pathological section is rich in gastric glands that are closely arranged with a normal structure, and the gastric gland epithelial cells have a normal morphology. In the model group, the lamina propria were loosely arranged, the lamina propria of the gastric mucosa was severely congested (black arrow), and there were a large number of inflammatory cells (blue arrow) under the mucosa with edema, as shown in Fig 2B.

### Chromatogram in total ion mode

The components separated by chromatography entered into mass spectrometry (MS) analysis, and data collection was performed by continuous scanning of the mass spectrum. The intensity is on the ordinate, and the time is on the abscissa. The resulting spectrum is the base peak chromatogram (BPC); see Fig 3A and 3B (G: model group, H: control group).

### Urine metabolomics analysis in positive ion mode

After data pretreatment (format conversion peak recognition, filtering alignment and normalization), the data screened out have strong repeatability and good effect for urine metabolomics analysis. After the data were preprocessed, the principal component analysis (PCA) method was used to explore CAG urine in positive ion mode. Changes in the fluid metabolism profile yielded a model with three principal components ( $R^2 = 0.548$ ) and a score chart reflecting the degree of dispersion between groups, as shown in Fig 4A. The PCA score graph shows that most samples are within the ellipse of the 95% confidence interval except for individual outliers. The PCA score graph shows that the urine samples of the two groups are significantly separated and are statistically significant. Furthermore, PLS-DA and OPLS-DA analysis methods (Fig 4B and 4C) were used to remove information that was not related to sample classification, and pattern discrimination analysis was performed on the full spectrum of the urine. Permutation is the result of 200 permutation tests, PLD-DA permutation test in positive ion mode is  $R^2 = (0.0, 0.91)$ ,  $Q^2 = (0.0, 0)$  PLD-DA permutation test in negative ion mode is  $R^2 = (0.0, 0.9)$ ,  $Q^2 = (0.0, -0.39)$ . The results showed that the two groups of samples could be significantly separated. In order to check whether the repeatability of the model is good and ensure the reliability of the data model, a permutation test was performed on the model (Fig 4D). The above results show that the multivariate data model of urine samples meets the parameter standard, indicating that the model has high stability and good predictive ability.

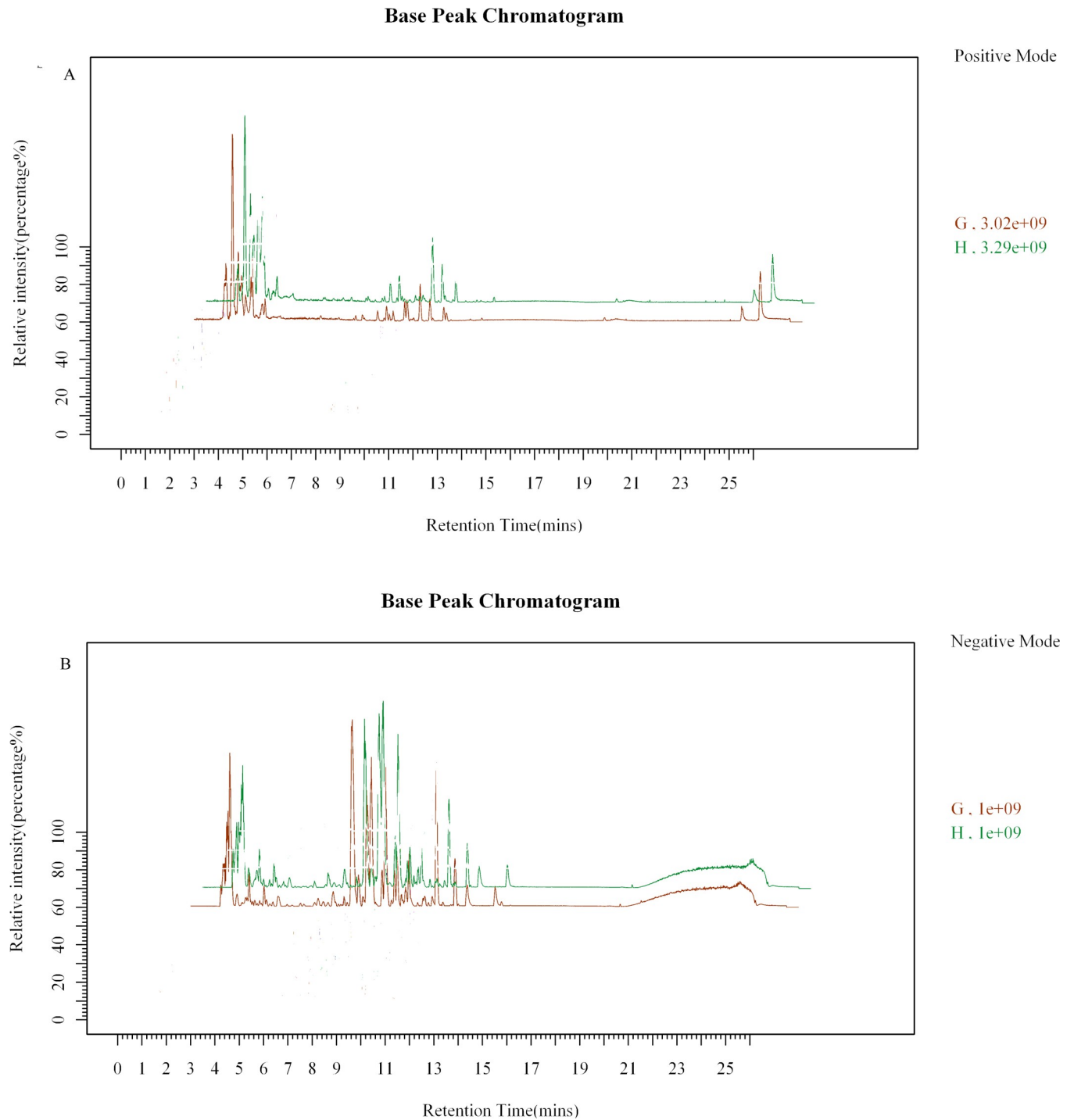


**Fig 3. Chromatogram in total ion mode.** 3-A: Typical Sample BPC in Positive Ion Mode, 3-B: Typical Sample BPC in Negative Ion Mode.

<https://doi.org/10.1371/journal.pone.0236203.g003>

### Analysis of urine metabolomics in negative ion mode

The PCA method was used to explore changes in the CAG urine metabolic spectrum. After data preprocessing, a model with 3 principal components ( $R^2 = 0.515$ ) and the degree of dispersion between groups were obtained from the score chart. The PCA score graph shows that

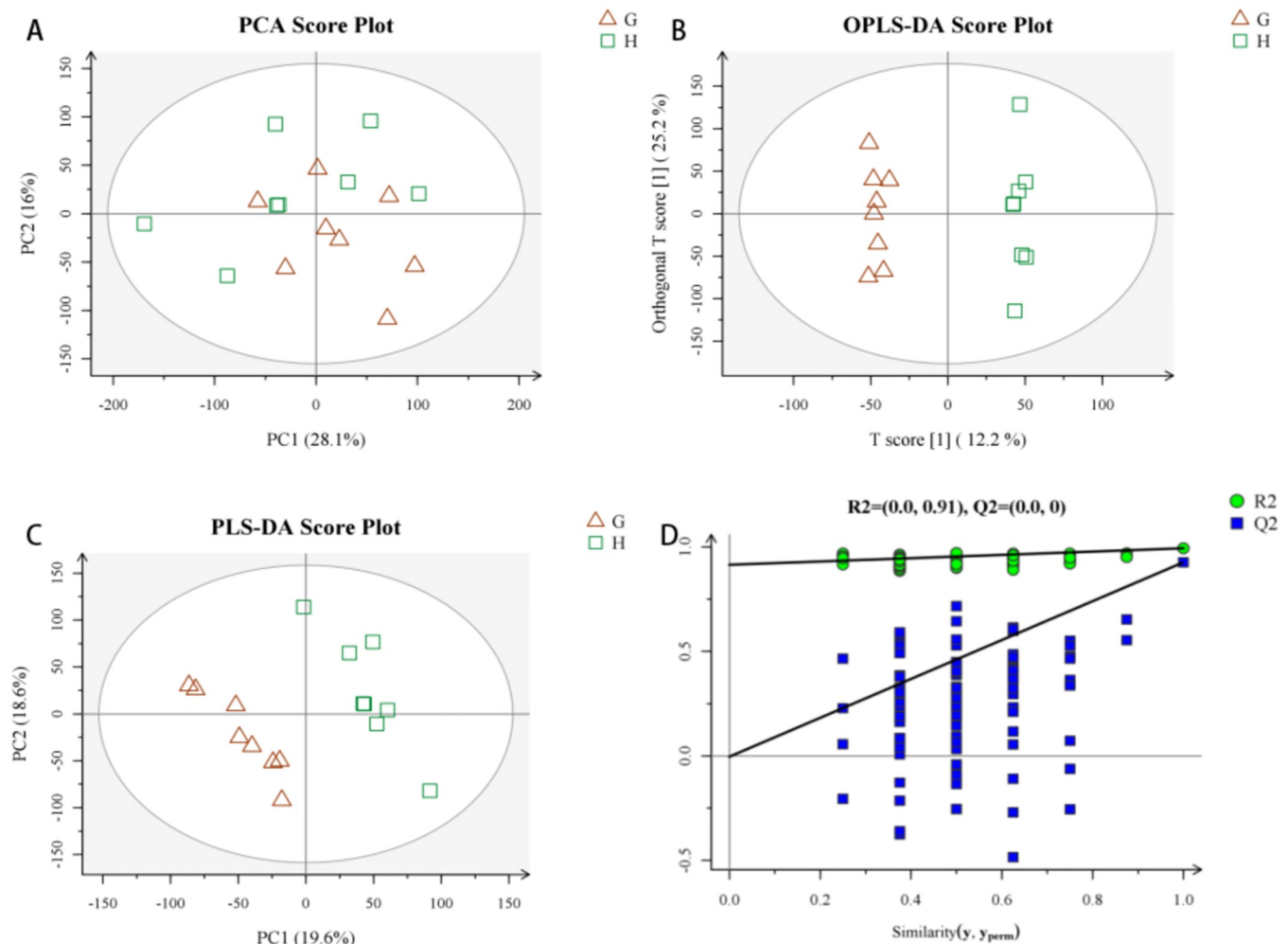


**Fig 4. Urine metabolism profile of CAG model rats in positive ion mode.** 4-A: PCA Scores, 4-B: PLS-DA Scores, 4-C: OPLS-DA Scores, 4-D: Replacement Test of the CAG Model Urine Fit Model in Positive Ion Mode.

<https://doi.org/10.1371/journal.pone.0236203.g004>

most samples fall within the ellipse of the 95% confidence interval, with only a few outliers. The PCA score (Fig 5A) graph shows the spatial distribution of the urine samples of the two groups, which can be significantly separated. PLS-DA and OPLS-DA analysis methods were used to further analyze the full spectrum of urine, and the results showed that the two groups of samples could be significantly separated (Fig 5B and 5C). In order to test whether the repeatability of the model is good and to ensure reliability of the data model, the model was replaced and verified (Fig 5D). The intercept of Q2 is negative, indicating that the model is valid. The above results indicate that the multivariate data model of urine samples meets the parameter standard, indicating that the model has high stability and good predictive ability.

### Extraction and analysis of differential metabolites

From the PCA, PLS-DA, OPLS-DA analysis model group and blank group, the screening conditions were in accordance with a P-value  $\leq 0.05$ ,  $VIP \geq 1$  [6], and molecular weight error  $< 20$  ppm). According to the fragmentation information obtained from MS/MS mode, further matching annotations were obtained in the HMDB, METLIN, MassBank, LipidMaps, and

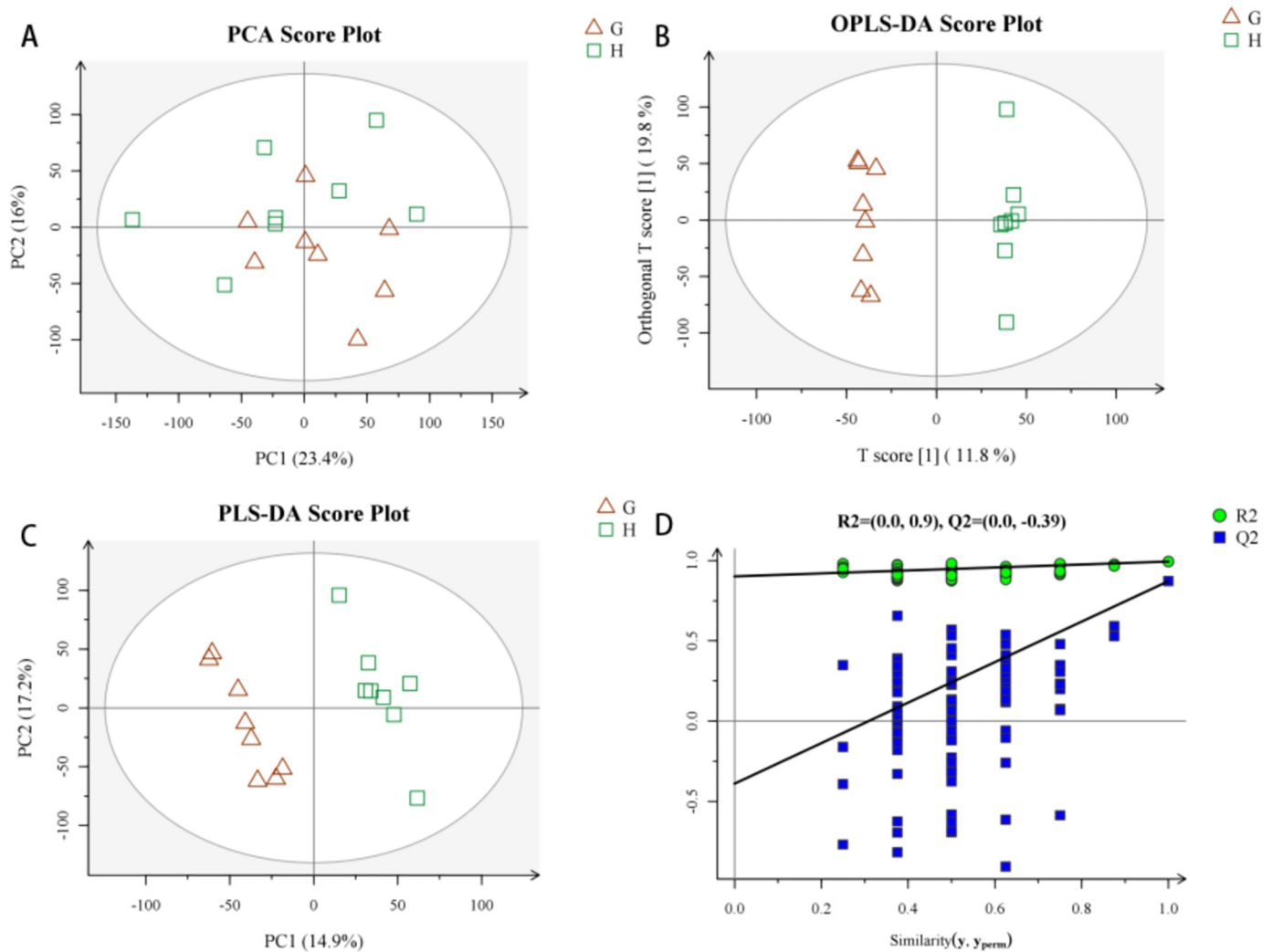


**Fig 5. Urine metabolism profile of CAG model rats in negative ion mode.** 5-A: PCA Scores, 5-B: PLS-DA Scores, 5-C: OPLS-DA Scores, 5-D: Replacement Test of the CAG Model Urine Fit Model in Negative Ion Mode.

<https://doi.org/10.1371/journal.pone.0236203.g005>

mzCloud databases to obtain accurate metabolite information. A total of 68 differential metabolites were screened, of which 25 were upregulated and 43 that were downregulated, compared with metabolites with the same or similar metabolic modes clustered to obtain differential metabolite heat maps and metabolite correlation heat maps (Fig 6). These differential metabolites relied on the Marker-view, KEGG, HMDB, MetaboAnalyst and other databases, which were searched and identified, and the results are shown in Table 1.

### CAG model group urine differential metabolite pathway information

This study mapped the differential metabolites to the KEGG database. There are 23 common metabolic pathways involved in the obtained differential metabolites, as shown in Fig 7: D-glutamine and D-glutamine histidine metabolism, histidine metabolism, purine metabolism, nitrogen metabolism, tyrosine metabolism, arginine-proline metabolism, butyric acid metabolism, biotin metabolism, alanine-aspartic acid-glutamic acid metabolism, ascorbic acid-bitter almond metabolism, niacin-nicotinamide metabolism, pentose-glucuronate interconversion,



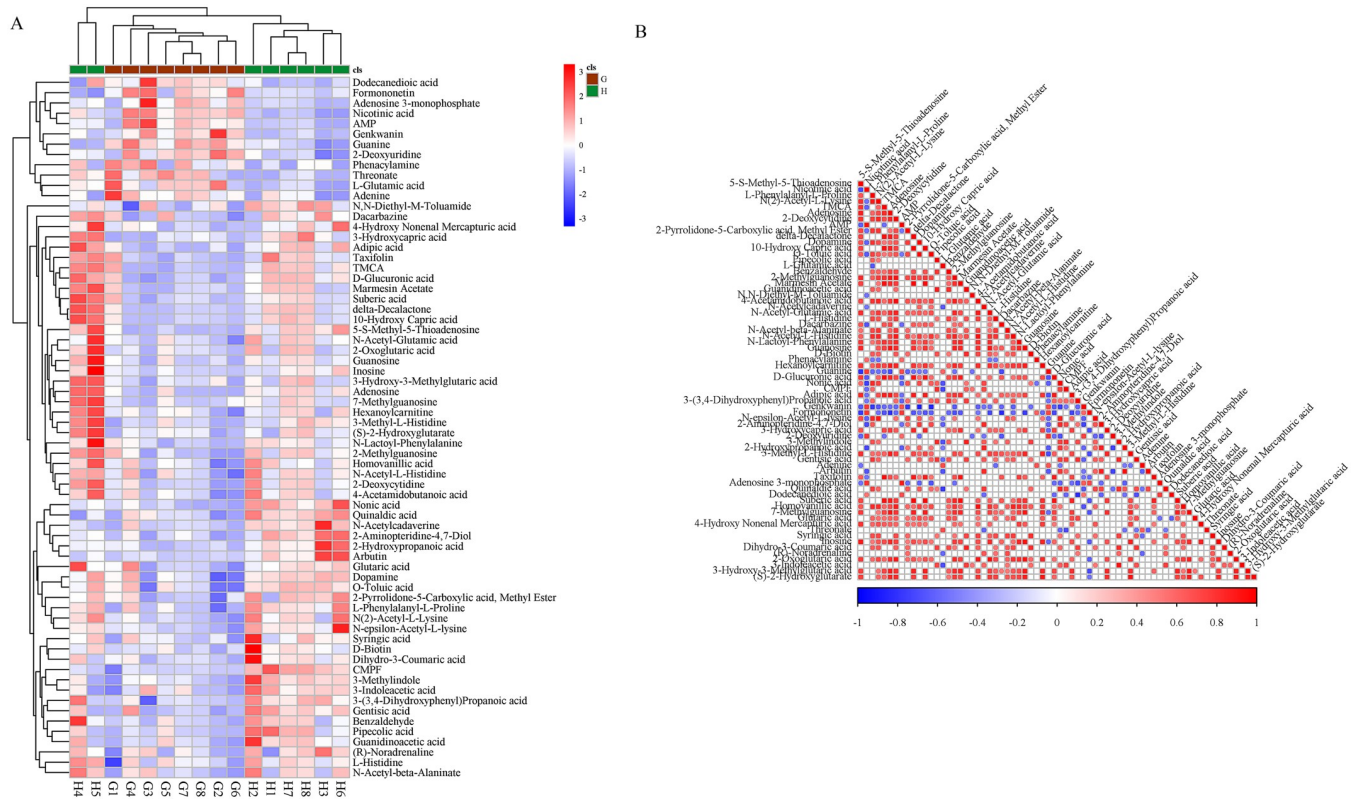


**Fig 6. Heat map of the differential metabolites.** A: Heat Map of the Differential Metabolites in CAG Rats; 6-B: Correlation Heat Map of Differential Metabolites in CAG Rats.

<https://doi.org/10.1371/journal.pone.0236203.g006>

pyrimidine metabolism, lysine degradation, citric acid cycle (TCA cycle), starch-sucrose metabolism, Inositol phosphate metabolism, glutathione metabolism, porphyrin and chlorophyll metabolism, cysteine-methionine metabolism, glycine-serine-threonine metabolism, aminoacyl-tRNA biosynthesis, and tryptophan metabolism. Among them, the metabolic pathways with  $P < 0.5$  and  $Impact > 0$  include D-glutamine and D-glutamic acid metabolism, histidine metabolism, and purine metabolism, as shown in Table 2. In these pathways, D-glutamine and D-glutamic acid metabolism were up-regulated, three metabolites in histamine metabolism were down-regulated, and six metabolites in purine metabolism were down-regulated.

### Discussion

In recent years, metabolomics has been widely used in modern Chinese medicine treatment of chronic gastritis. Cui Jiajia Et al. [8] found that 3 plasma biomarkers (arginine, succinate and 3-hydroxybutyrate) and 2 urine biomarkers ( $\alpha$ -ketoglutarate and valine) might be markers of CAG in the study on plasma and urine metabolites. Chen jiaolong [9] by using nuclear magnetic metabolomics technology including observation of the stomach meridian the CAG treatment, use of electroacupuncture in the rat stomach meridians beam door and foot three mile, found that serum ghrelin level stomach metabolism of liver kidney brain cortex spectral change, the rat gastric mucosa arrangement and the thickness of the gastric mucosa has different degrees of improvement, ghrelin and substance P expression in serum increased to normal level, serum glucose glycogen content increased, the stomach tissue of glutathione and

**Table 1. Differential metabolic markers in urine of CAG rats (upregulated ↑, downregulated ↓).**

chemical compound	m/z	rt	exact mass	chemical formula	Model vs Control_VIP	log <sub>2</sub> (FC)	p value
(S)-2-Hydroxyglutarate	147.0287633	82.9724	148.11402	C5H8O5	1.464880663	0.5013	0.047581863↓
<sup>®</sup> -Noradrenaline	184.0967985	330.939	183.205	C8H11NO3	1.526685758	0.3797	0.037595251↓
10-Hydroxy capric acid	189.1483988	609.2975	188.264	C10H20O3	1.823597606	1.5684	0.008306808↑
2-Aminopteridine-4,7-Diol	178.0362164	219.251	179.1364	C6H5N5O2	2.016289866	1.1144	0.003043425↑
2-Deoxycytidine	228.0976635	149.877	227.2172	C9H13N3O4	1.915004809	1.3307	0.004840515↑
2-Deoxyuridine	227.0667048	283.209	228.202	C9H12N2O5	1.943477192	-0.979	0.004861136↓
2-Hydroxypropanoic acid	89.02311403	93.0333	90.0779	C3H6O3	1.874058772	0.3997	0.00731866↓
2-Methylguanosine	298.1143794	220.051	297.2675	C11H15N5O5	1.751775025	1.367	0.012215874↑
2-Oxoglutaric acid	145.0131155	83.6063	146.0981	C5H6O5	1.495118055	0.9552	0.042475723↓
2-Pyrrolidone-5-Carboxylic acid, Methyl Ester	144.0654693	163.765	143.0582432	C6H9NO3	1.868632508	0.4193	0.006413493↓
3-(3,4-Dihydroxyphenyl)Propanoic acid	181.0496532	227.9005	182.1733	C9H10O4	2.070984986	0.8642	0.002077192↓
3-Hydroxy-3-methylglutaric acid	161.044468	84.9492	162.1406	C6H10O5	1.480741362	0.7542	0.044849483↓
3-Hydroxycapric acid	187.1330551	667.4145	188.264	C10H20O3	1.944065438	0.3836	0.004843594↓
3-Indoleacetic acid	174.0550606	463.637	175.184	C10H9NO2	1.490647745	0.5842	0.043203485↓
3-Methylindole	130.0650034	464.003	131.1745	C9H9N	1.876426797	0.9857	0.007221167↓
3-Methyl-L-histidine	168.0767831	105.457	169.18126	C7H11N3O2	1.872481394	1.4212	0.00738418↑
4-Acetamidobutanoic acid	146.0811334	296.814	145.15648	C6H11NO3	1.641325837	0.526	0.02089112↓
4-Hydroxy nonenal Mercapturic acid	318.1376294	559.432	319.1453439	C14H25NO5S	1.548812817	1.0965	0.034435408↑
5-S-Methyl-5-thioadenosine	298.0965219	450.365	297.3347	C11H15N5O3S	2.284849647	1.8528	0.000234115↑
7-Methylguanosine	296.0994864	384.98	297.1073186	C11H16N5O5	1.568140916	1.549	0.031843615↑
Adenine	134.0460176	301.647	135.1269	C5H5N5	1.792987662	-0.7032	0.011340028↓
Adenosine	268.1038713	289.983	267.24152	C10H13N5O4	1.934286006	2.0713	0.004285334↑
Adenosine 3-monophosphate	346.0554562	184.5985	347.22142	C10H14N5O7P	1.68169368	-1.3227	0.019481197↓
Adipic acid	145.049496	93.721	146.1412	C6H10O4	2.113128751	1.3866	0.001516902↑
AMP	348.0700631	175.3335	347.2212	C10H14N5O7P	1.900260783	-1.5778	0.005302741↓
Arbutin	271.0820178	255.116	272.2512	C12H16O7	1.771574784	2.3461	0.012648447↑
Benzaldehyde	107.0492548	441.291	106.1219	C7H6O	1.762739968	1.0398	0.011540491↑
CMPF	239.0910035	181.3095	240.2524	C12H16O5	2.124552651	1.2416	0.001388456↑
Dacarbazine	183.1015094	706.8775	182.18344	C6H10N6O	1.587732534	0.2827	0.026523445↓
D-Biotin	245.0919668	518.395	244.31172	C10H16N2O3S	1.515098427	1.0857	0.035928770↑
delta-Decalactone	171.1378437	609.401	170.2487	C10H18O2	1.849847045	1.5177	0.007156206↑
D-Glucuronic acid	193.0345141	562.589	194.1394	C6H10O7	2.241280415	1.2756	0.000512579↑
Dihydro-3-coumaric acid	165.0546401	410.747	166.1739	C9H10O3	1.528214666	1.394	0.037370134↑
Dodecanedioic acid	229.1439549	580.91	230.30068	C12H22O4	1.66119894	-0.9546	0.021378107↓
Dopamine	154.0861938	172.7845	153.1784	C8H11NO2	1.825498392	0.753	0.008218865↓
Formononetin	267.066017	806.608	268.2641	C16H12O4	2.025071834	-1.1042	0.002867682↓
Genkwanin	283.0608516	871.0265	284.2635	C16H12O5	2.062070851	-1.1857	0.002214871↓
Gentisic acid	153.0181962	231.027	154.12014	C7H6O4	1.835909917	1.2406	0.009038573↑
Glutaric acid	131.0337596	93.248	132.11462	C5H8O4	1.55606035	0.6234	0.033445496↓
Guanidinoacetic acid	118.0613176	92.6126	117.107	C3H7N3O2	1.705152566	1.0027	0.015441198↑
Guanine	150.0409746	176.319	151.126	C5H5N5O	2.476437968	-1.3203	3.25E-05↓
Guanosine	284.0987672	329.596	283.24092	C10H13N5O5	1.53671651	1.3507	0.032900583↑
Hexanoylcarnitine	260.1854318	582.32	259.1783583	C13H25NO4	1.466692106	0.5425	0.043469353↓
Homovanillic acid	181.0496668	326.991	182.1733	C9H10O4	1.602561332	0.5841	0.027598265↓
Inosine	267.0731584	331.1715	268.2261	C10H12N4O5	1.528975498	2.1558	0.037258488↑
L-Glutamic acid	148.0602887	91.7513	147.1293	C5H9NO4	1.777690879	-1.1167	0.010667276↓
L-Histidine	156.0766725	105.9695	155.15468	C6H9N3O2	1.603838417	0.5723	0.024721392↓

(Continued)

Table 1. (Continued)

chemical compound	m/z	rt	exact mass	chemical formula	Model vs Control_VIP	log2 (FC)	p value
L-Phenylalanyl-L-Proline	263.1388345	500.41	262.3043	C14H18N2O3	2.077282892	0.7931	0.001566615↓
Marmesin acetate	289.1019761	693.8425	288.0997736	C16H16O5	1.720421852	0.9461	0.014319362↓
N(2)-Acetyl-L-Lysine	189.1232505	106.081	188.22432	C8H16N2O3	2.049816081	0.8419	0.001930407↓
N,N-Diethyl-M-Toluamide	192.1381451	1046.76	191.2695	C12H17NO	1.658473782	0.6825	0.019299997↓
N-Acetyl-beta-Alaninate	132.065568	184.861	130.1219	C5H9NO3	1.573650573	0.5139	0.028179966↓
N-Acetylcadaverine	145.1334792	149.971	144.215	C7H16N2O	1.640234776	1.0602	0.020995681↑
N-Acetyl-Glutamic acid	190.0709275	195.285	189.1659	C7H11NO5	1.606367357	0.6886	0.024447196↓
N-Acetyl-L-Histidine	198.0872059	106.068	197.19136	C8H11N3O3	1.573531368	0.4979	0.028194318↓
N-epsilon-Acetyl-L-lysine	187.1078578	100.753	188.22432	C8H16N2O3	2.024611789	0.6354	0.00287668↓
Nicotinic acid	124.0394187	147.588	123.10944	C6H5NO2	2.168087639	-1.2801	0.000737259↓
N-Lactoyl-phenylalanine	238.1071057	597.55	237.100108	C12H15NO4	1.57132921	0.907	0.028460454↓
Nonic acid	187.0966503	487.9895	188.104859	C9H16O4	2.208499912	0.5276	0.000690754↓
O-Toluic acid	137.059717	171.166	136.14792	C8H8O2	1.805758215	0.7836	0.009169037↓
Phenacylamine	136.0745078	3.70776	135.0684139	C8H9NO	1.489849766	-0.4527	0.039727046↓
Pipecolic acid	130.0862919	132.1165	129.157	C6H11NO2	1.781759339	1.5181	0.010438908↑
Quinaldic acid	172.039368	306.26	173.1681	C10H7NO2	1.669168777	0.7797	0.020624237↓
Suberic acid	173.0809113	144.3395	174.19436	C8H14O4	1.612701672	1.3484	0.026434225↑
Syringic acid	197.0447419	256.6915	198.1727	C9H10O5	1.538159222	0.7057	0.035930624↓
Taxifolin	303.0519806	562.747	304.2516	C15H12O7	1.718717369	0.8785	0.016387198↓
Threonate	135.0287318	86.9696	136.10332	C4H8O5	1.547635686	-0.6082	0.034598259↓
TMCA	239.0887447	588.709	238.2366	C12H14O5	1.954028191	1.161	0.003771041↑

<https://doi.org/10.1371/journal.pone.0236203.t001>

glutamine levels, hypoxanthine creatinine nicotinamide in brain tissue The content of malonic acid and dimethyl malonate increased, the content of glucod carbonate and glycerin in liver tissues increased, and the content of glutamine hypoxanthine nucleoside asparagine asparagine and nicotinamide in kidney tissues increased. Liu Caichun Et al. [10] found that both

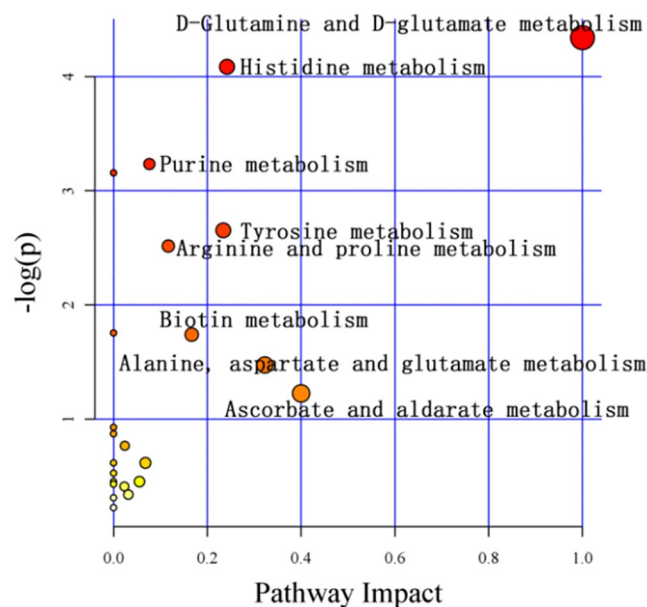


Fig 7. Metabolic pathways of CAG rat metabolites mapped to KEGG.

<https://doi.org/10.1371/journal.pone.0236203.g007>

Table 2. Differential metabolic pathways in urine of CAG rats.

	D-Glutamine and D-glutamate metabolism	Histidine metabolism	Purine metabolism
p value	0.013036	0.016826	0.039418
Impact	1	0.24194	0.076410
Pathway links	<a href="http://www.kegg.jp/pathway/rno00471+C00025+C00026">http://www.kegg.jp/pathway/rno00471+C00025+C00026</a>	<a href="http://www.kegg.jp/pathway/rno00340+C00025+C00135+C01152">http://www.kegg.jp/pathway/rno00340+C00025+C00135+C01152</a>	<a href="http://www.kegg.jp/pathway/rno00230+C00020+C00212+C00294+C00242+C00387+C00147">http://www.kegg.jp/pathway/rno00230+C00020+C00212+C00294+C00242+C00387+C00147</a>

<https://doi.org/10.1371/journal.pone.0236203.t002>

electroacupuncture and moxibustion could restore various caG-induced metabolic changes, including membrane metabolism, energy metabolism and neurotransmitter function. Liu Yuetao [11] based on 1 H-NMR technical analysis astragalus chienchung soup to the CAG rats serum endogenous metabolites regulation function disorder, through multivariate statistical analysis, to clarify its regulation on chronic atrophic gastritis targets, related indicators associated with efficacy is established, by partial least-squares regression analysis and Met PA screening and treatment effect is most related metabolic pathways, find the root of remembraneous milk vetch chienchung soup can obviously inhibit the CAG lesions, can obviously regulate 3—hydroxy butyric acid lactic acid acetate succinate metabolites such as disorder, the CAG treatment is the main metabolic pathways of arginine—proline metabolism Glycerol metabolism and glycine—serine—threonine metabolism pathways. Sun Yina [12] found 59 qualitative and quantitative metabolites, and then PCA OPLS-DA VIP value was used to find 8 potential differential metabolites related to dampis-heat syndrome of spleen and stomach. The metabolites of trimethyl-oxide of taurine gonosaccharide glycerol and glucose were up-regulated, and the metabolites of trimethyl-trimethyl-oxide and trigonelline phosphate creatine were down-regulated. It is concluded from the above studies that metabonomic techniques have been widely used in traditional Chinese medicine. However, 1H-NMR metabolism technology is mostly used in the studies on chronic atrophic gastritis. In this study, LC-MS technology is used to elucidate the small molecule action mechanism and related target pathways of CAG. In this study, the animal model of chronic atrophic gastritis was mainly prepared by MNNG combined with ammonia-free drinking water and hunger and satiety. The process of MNNG alkylating the DNA bases does not depend on enzymatic metabolism and can directly penetrate into the pylorus and stomach to cause canceration [13]. Alcohol can trigger acute ischemic damage to the gastric mucosa, causing damaged genes to fail to recover over time, which may be an important factor for initiating oncogenes [14]. Moreover, alcohol can accelerate the dissolution of MNNG and increase the mutation rate. Ammonia can simulate toxic damage to the stomach after *Helicobacter pylori* infection and maintain acute inflammation of the gastric mucosa [15, 16]. Ranitidine hydrochloride can inhibit gastric acid secretion, but hunger and satiety are the fusion of spleen and stomach damage. CAG is a complex disease with multiple factors and multiple genes. Compound factor modeling can simulate human disease characteristics to a greater extent and is currently the most widely used and most mature CAG model application.

Through PCA, PLS-DA and OPLS-DA LC-MS diversified analysis, using statistics, bioinformatics, chemometrics and other methods to analyze and compare the differential metabolites, the model group and the blank group of rat urine had significant metabolic differences. A total of 68 different metabolites were screened, and 23 metabolic disturbance pathways were predicted. The metabolic pathways can regulate the growth, differentiation, apoptosis and the immune system of tumor cells [17]. The statistically significant metabolic pathways are D-glutamine and D-glutamic acid metabolism, histidine metabolism, and purine metabolism. Among the metabolic pathways, the significantly different metabolites included L-glutamic

acid and 10 different products, including ketoglutaric acid, histidine, 3-methyl-L-histidine, adenosine monophosphate, adenosine, adenine, hypoxanthine, guanosine and guanine.

L-Glutamic acid, which is in the metabolic pathway of D-glutamine and D-glutamic acid, plays an important role in protein metabolism in organisms. Studies have found that L-glutamic acid can inhibit cerebral cortex, hippocampal, gastric cancer cell and neural stem cell proliferation and differentiation and induce apoptosis [18, 19]. Decreased glutamate expression levels will cause digestive system diseases. Based on this performance, L-glutamic acid is a commonly used therapeutic drug for the digestive system, especially gastric cancer and pancreatic cancer. Penicillin can induce the generation of glutamic acid and upregulate cycle-related expression genes and sugar degradation process of glucose to 2-oxoglutaric acid [20].

In the histidine metabolism pathway, 3-methyl-L-histidine, histidine, and L-glutamic acid play the role of substrate, intermediate, and product, respectively, and protein nutrition comes from the content of 3-methyl-L-histidine. Each of these compounds are effective indicators of histidine metabolic status [21]. Studies have confirmed that histidine can inhibit the proliferation and migration of lung cancer cells, thereby exerting an antitumor effect [22]. Histamine formed after the decarboxylation of histidine can relax blood vessels and is associated with inflammation. In gastritis and in the duodenum, the reaction in ulcers is sensitive. Currently, histidine is mostly used for the treatment of reducing gastric acid, relieving gastrointestinal pain and as a blood pressure treatment. L-Glutamic acid is formed after a series of processes, such as phosphoester and propionic acid formation, and its antagonists can reverse the abnormal expression of mGlu R5 and PSD-95 in the striatum of LID rats [23].

Purine metabolism provides cells with the necessary energy and cofactors to promote the growth and proliferation of cells. The most common disease with purine dysfunction is gout, and purine metabolism and its metabolites include adenosine monophosphate, adenosine, adenine, and, at times, the abnormal expression of xanthine, guanosine and guanine will promote the occurrence of gastric cancer [24]. The decomposition of purine nucleotides will promote the dephosphorylation of inosine or guanylic acid and generate inosine or guanosine, which can decompose into xanthine or guanine. The CN-II enzyme is highly expressed in tumor cells [25]. Studies have shown that purine nucleotides are essential for metabolic functions. Hypoxanthine, guanine phosphoribosyl transferase and other related purines can affect hematopoietic stem cell cycle progression, proliferation kinetics and changes in mitochondrial membrane potential [26].

## Conclusions

Metabolomics is an important technical means for studying the pathogenesis of diseases. This experiment is the first to use LC-MS metabolomics to study the pathogenesis of CAG from the perspective of urine metabolites. From the method (PCA) and supervised analysis method (PLS-DA and OPLS-DA), differential metabolites of the model group and the control group were screened. These differences were mainly distributed among 23 metabolic pathways, which were glutamine metabolism with L-glutamic acid, 2-ketoglutarate in the D-glutamic acid metabolism pathway, 3-methyl-L-histidine, histidine, L-glutamic acid and purine in the histidine metabolism pathway. Adenosine monophosphate, adenosine, adenine, inosine, guanosine and guanine may be potential biomarkers for the diagnosis of CAG.

## Supporting information

**S1 Checklist.** *PLOS ONE* humane endpoints checklist.  
(DOCX)

## Acknowledgments

The authors thank Suzhou BioNovoGene Biopharmaceutical Technology Co., Ltd., for their technical assistance. And the Editing and Manuscript Formatting service provided by American Journal Experts.

## Author Contributions

**Data curation:** Guo-Xiu Zu, Qian-Qian Sun.

**Formal analysis:** Ling Li, Hai-Liang Huang.

**Funding acquisition:** Tao Han.

**Investigation:** Liang-Kun Zhang.

**Methodology:** Guo-Xiu Zu, Qian-Qian Sun, Jian Chen, Ling Li.

**Project administration:** Xi-Jian Liu.

**Supervision:** Ke-Yun Sun, Hai-Liang Huang.

**Visualization:** Ke-Yun Sun.

**Writing – original draft:** Guo-Xiu Zu.

**Writing – review & editing:** Jian Chen, Xi-Jian Liu, Liang-Kun Zhang, Tao Han, Hai-Liang Huang.

## References

1. Jiang Y, Qi X, Liu X, Zhang J, Ji J, Zhu Z, et al. Fbxw7 haploinsufficiency loses its protection against DNA damage and accelerates MNU-induced gastric carcinogenesis. *Oncotarget*. 2017; 8: 33444–33456. <https://doi.org/10.18632/oncotarget.16800> PMID: 28422719
2. Hao H. Correlation between pathological classification of chronic atrophic gastritis patients and TCM constitution types. Shanxi Provincial Institute of Traditional Chinese Medicine; 2017.
3. Wu Q. CKD-MBD related biomarkers based on metabolomics biological screening and research on the toxicity mechanism of bone metabolism. Second Military Medical University; 2017.
4. Hu T. Research on new methods and strategies for the analysis of endogenous lipid compounds based on chromatographic mass spectrometry. Peking Union Medical College; 2018.
5. Kong XR, Yang Y, Li HZ, Liu L, Zhao SM, Liu HY, et al. The effect of different routes and doses of N-methyl-N-nitro N-nitrosoguanidine administration on pathological changes of gastric mucosa in rats. *Chin J Integr Tradit West Med Dig*. 2015; 23: 381–384, 389.
6. Want EJ, Masson P, Michopoulos F, Wilson ID, Theodoridis G, Plumb RS, et al. Global metabolic profiling of animal and human tissues via UPLC-MS. *Nat Protoc*. 2013; 8: 17–32. <https://doi.org/10.1038/nprot.2012.135> PMID: 23222455
7. Smith CA, Want EJ, O'Maille G, Abagyan R, Siuzdak G. XCMS: processing mass spectrometry data for metabolite profiling using nonlinear peak alignment, matching, and identification. *Anal Chem*. 2006; 78: 779–787. <https://doi.org/10.1021/ac051437y> PMID: 16448051
8. Cui Jiajia et al. "NMR-based metabolomics and correlation analysis reveal potential biomarkers associated with chronic atrophic gastritis". 132(2017):77–86.
9. Jiaolong Chen. Metabolomics based study on the mechanism of electroacupuncture in the treatment of chronic atrophic gastritis [D]. Fujian University of Traditional Chinese Medicine, 2018.
10. Liu Cai-chun, et al. "Comparative metabolomics study on therapeutic mechanism of electro-acupuncture and moxibustion on rats with chronic atrophic gastritis (CAG)." *Scientific Reports* 7.1 (2017): 1–11.
11. Liu YueTao, et al. "Urinary metabolomics research for Huangqi Jianzhong Tang against chronic atrophic gastritis rats based on 1H NMR and UPLC-Q/TOF MS." *Journal of Pharmacy and Pharmacology* 72.5 (2020): 748–760. <https://doi.org/10.1111/jphp.13242> PMID: 32128823
12. Yina Sun. Pathogenesis transformation of spleen and stomach dampness-heat syndrome of Hp gastritis and its metabolomics study [D]. Hubei University of Chinese Medicine, 2017.

13. Qi X, et al. Experimental study on the effect of MNNG compound method on the model of gastric precancerous lesions on inflammatory factors. *Hubei J Tradit Chin Med*. 2019; 41: 3–4.
14. Yuan X. Research progress of rat models of precancerous lesions. *J Anhui Tradit Chin Med Coll*. 2004; 23: 62–64.
15. Si J, Wu J, Cao Q, Zun JL. Establishment of rat model of chronic atrophic gastritis discussion on the factors of atrophy. *Chin J Dig*. 2001: 7–10.
16. Geng Z, Huang Y, Chen J. Experimental study on the effect of Taibai rice n-butanol extract on chronic gastritis in rats. *Jilin Zhong Med*. 2009; 29: 527–528.
17. Wei J, Wu A, Kong LY, Wang Y, Fuller G, Fokt I, et al. Hypoxia potentiates glioma-mediated immunosuppression. *PLoS One*. 2011; 6: e16195.
18. Gao C, Wang J, Zhou X. Changes of neuronal apoptosis in rat model of kidney yin deficiency induced by L-monosodium glutamate. *Chin J Med*. 2003: 719–720.
19. Gao S, Wang J. Changes of neural stem cell proliferation and differentiation-related proteins in L-monosodium glutamate rats. *J Third Mil Med Univ*. 2004: 1524–1526.
20. Hirasawa T, Saito M, Yoshikawa K, Furusawa C, Shmizu H. Integrated analysis of the transcriptome and metabolome of *Corynebacterium glutamicum* during penicillin-induced glutamic acid production. *Biotechnol J*. 2018; 13: 1700612.
21. Chen D, et al. Amino acid analyzer for rapid determination of 3-methylhistidine in urine. *Sichuan J Physiol Sci*. 1988: 56–57.
22. Escobar-Reséndiz R, Reyes-Esparza J, Blake IO, Rodríguez-Fragoso L. Evaluation of antitumoral effect of the combination of L-histidine methyl ester hydrochloride of anferic B with antineoplastics on A549 cells. *FASEB J*. 2020; 34: 1.
23. Shu H. Experimental study on the effect of metabolic glutamate receptor 5 antagonist MPEP on rats with levodopa-induced Parkinson's disease dyskinesia. Suzhou University; 2015.
24. Feng X, Ma D, Zhao J, Song Y, Zhu Y, Zhou Q, et al. UHMK1 promotes gastric cancer progression through reprogramming nucleotide metabolism. *EMBO J*. 2020; 39: e102541.
25. Tozzi MG, Pesi R, Allegrini S. On the physiological role of cytosolic 5'-nucleotidase II (cN-II): pathological and therapeutical implications. *Curr Med Chem*. 2013; 20: 4285–4291. <https://doi.org/10.2174/0929867311320340007> PMID: 23992310
26. Vogel M, Moehrle B, Brown A, Eiwien K, Sakk V, Geiger H. HPRT and purine salvaging are critical for hematopoietic stem cell function. *Stem Cells*. 2019; 37: 1606–1614. <https://doi.org/10.1002/stem.3087> PMID: 31574190